Supplementary Information for hybrid brightfield and darkfield transport of intensity approach for high-throughput quantitative phase microscopy

Linpeng Lu,[†,†,¶,§,‖] Jiaji Li,[‡,†,¶,§,‖] Yefeng Shu,[‡,†,¶,§] Jiasong Sun,[‡,†,¶,§] Jie Zhou,[‡,†,¶,§] Edmund Y. Lam,[*,⊥] Qian Chen,[*,‡,¶] and Chao Zuo[*,‡,†,¶,§]

†*Smart Computational Imaging Laboratory (SCILab), Nanjing University of Science and Technology, Nanjing, Jiangsu Province 210094, China*

‡*School of Electronic and Optical Engineering, Nanjing University of Science and Technology, No. 200 Xiaolingwei Street, Nanjing, Jiangsu Province 210094, China*

¶*Jiangsu Key Laboratory of Spectral Imaging & Intelligent Sense, Nanjing, Jiangsu Province 210094, China*

§*Smart Computational Imaging Research Institute (SCIRI) of Nanjing University of Science and Technology, Nanjing, Jiangsu Province 210019, China*

‖*Equal contributor*

⊥*Department of Electrical and Electronic Engineering, The University of Hong Kong, Pokfulam, Hong Kong SAR, China*

E-mail: zuochao@njust.edu.cn; chenqian@njust.edu.cn; elam@eee.hku.hk

Abstract

This document provides supplementary information to the "Hybrid brightfield and darkfield transport of intensity (HBDTI) approach for high-throughput quantitative phase microscopy". We present more details including the principle and quantification analysis, a comparison with different quantitative phase imaging techniques, the analysis of the data collection procedure and the number of iterations, the LED illumination chosen strategy, and HBDTI MATLAB source code and datasets.

Contents

1. Principle
2. Comparison of different QPI techniques
3. Analysis of the data collection procedure
4. Analysis of the number of iterations
5. LED illumination strategy
6. Quantification and analysis of HBDTI
7. HBDTI MATLAB source code and datasets

1. Principle

In a typical microscopic imaging system, the image formation can be described by Fourier transforms and a linear filtering operation in the pupil plane. For coherent imaging systems, it is linear in complex amplitude, while linear in intensity for incoherent imaging systems. But the image formation in partially coherent systems is not linear in either amplitude or intensity but is bilinear, making phase recovery complicated [19, 25]. To simplify the mathematical formulation, strict assumptions such as paraxial approximation [15] and weak defocusing [23] are often applied to linearize the transport of intensity equation (TIE) phase retrieval. Then, quantitative phase distributions are retrieved by Fourier space deconvolution directly to decouple the solution from the linearized model [25].

Due to the neglect of partial coherence and the introduction of strict assumptions in the linearized imaging model, the tradeoff between resolution and field of view (FOV) cannot be overcome in the original TIE methods [15]. Since the image formation model transforms into a nonlinear inverse problem under non-paraxial condition, the darkfield (DF) imaging formation cannot be solved by TIE because of model mismatch. Consequently, the illumination source used in the existing TIE-based quantitative phase imaging (QPI) methods is usually limited to brightfield (BF) illumination, and it is not compatible with the DF illumination that provides high-resolution diffraction features. For this reason, high-throughput TIE-based QPI over the incoherent diffraction-limited resolution has not been reported so far. To address the contradiction between resolution and FOV in TIE-related QPI approaches, the forward imaging model of HBDTI is established to depict the captured intensity that takes into account the effect of partial coherence on the nonlinear imaging model, thereby incorporating DF illumination to extend the accessible object frequency.

In actual situations, BF intensity images usually have several orders of magnitude higher intensity than DF intensity images, and the noise of BF intensity may drown out the DF intensity signal. Considering the magnitude difference in BF and DF intensity images, it needs to measure the intensity images separately in these two modes for a better signal-to-noise ratio (SNR). Thus, HBDTI uses an iterative strategy to recover the phase from two sets of intensity measurements captured at different heights under BF and DF illuminations. By utilizing a low-numerical aperture (NA) objective, HBDTI obtains two through-focus intensity stacks corresponding to the BF and DF illuminations through a programmable light-emitting-diode (LED) array (Step 1). In Step 2, the captured in-focus intensity is

upsampled and combined with the zero-value phase for the initialization of high-resolution object complex amplitude U.

Considering the physical model of intensity transport, the coherent mode decomposition method is introduced to model the partially coherent optical field [34]. The low-resolution intensity measurements obtained under partially coherent illumination can be used to constrain the calculated intensity images under corresponding BF and DF patterns. Thus, in Step 3, a series of high-resolution through-focus intensity stacks are obtained by numerical propagation under corresponding LED illumination angles. After the downsampling of pixel binning, the calculated low-resolution intensity images can be treated as the input of the intensity constraints process. For a finite set of illumination vectors $\mathbf{u}_i = (u_x, u_y), i = 1, 2, ..., N$, the image formation of each intensity can be represented as

$$I_i^{cal}(\mathbf{r}) = \left|\mathscr{F}^{-1}\left\{P(\mathbf{u})\, O(\mathbf{u} - \mathbf{u}_i)\right\}\right|^2, i = 1, 2, ..., N, \tag{1}$$

where $\mathbf{r}$ is the real-space coordinate vector, $\mathscr{F}$ is the two-dimensional Fourier transform. $O(\mathbf{u})$ represents the Fourier transform of the object function, firstly shifted by the illumination vector $\mathbf{u}_i$, then confined by the pupil function $P(\mathbf{u})$, and finally inverse Fourier transform back to the real space to form in-focus high-resolution images $I_i^{cal}(\mathbf{r})$ corresponding to different illumination angles. The angular spectrum method is applied for the decomposed intensity images in the case of various illumination angles, obtaining the through-focus intensity stacks.

Then, in Step 4, two through-focus intensity stacks I_{BF}^{cal} and I_{DF}^{cal} corresponding to the BF (contains n LEDs) and DF (contains $N - n$ LEDs) illumination cases under the same defocus distance can be obtained through a superposition of intensities produced by mutually incoherent points of the corresponding illumination angles [39],

$$I_{BF}^{cal} = \sum_{i=1}^{n} I_i^{cal}, \tag{2}$$

$$I_{DF}^{cal} = \sum_{i=n+1}^{N} I_i^{cal}. \tag{3}$$

The measured intensity stacks are divided by the two stacks, and their square root versions are used as the factor to update the complex amplitude corresponding to various defocus

distances. For the recovery of objective function $O(\mathbf{u})$, most of the existing algorithms have been proposed by converting Eq. 1 into an optimization problem, and the corresponding vectorized objective function is as follows

$$\varepsilon = \sum_i \left\| \sqrt{\mathbf{I}_i} - \left| \mathbf{F}^{-1}\mathbf{P}_i\mathbf{O} \right| \right\|^2 \equiv \sum_i \left\| \sqrt{\mathbf{I}_i} - \left| \mathbf{g}_i \right| \right\|^2, \tag{4}$$

where $\|\cdot\|$ is the Euclidean norm, $\mathbf{F}$ is the matrix representation of the discrete Fourier transform and $\mathbf{g}_i = \mathbf{F}^{-1}\mathbf{P}_i\mathbf{O}$. The image and object function can be expressed as a vector $\mathbf{I}_i = \left\{ \mathrm{I}_{i,m}^{cal} \right\}_{m=1}^{M}$ and $\mathbf{O} = \{O_m\}_{m=1}^{L}$. Matrix $\mathbf{P}_i$ is $M \times L$ determined by $P(\mathbf{u})$, which extracts the sub-spectrum containing M pixels from the entire L pixels. The error metric given by Eq. 4 is real-space error, quantifying how closely the estimated value fits the input data.

Inspired by the strategy of Fourier ptychographic microscopy (FPM) [33], we apply the schemes of synthetic aperture and multiplexing to difference map [41, 44], which attempts to update the entire objective function in each iteration and finally converge to a more balanced globally consistent solution. Therefore, a high-resolution complex amplitude can be recovered by introducing high-resolution features from the DF intensity constraints, which contain sub-diffraction-limit sized characteristics. The following description is based on non-convex set projection theory to analyze difference map DM more intuitively, which is formed by the difference of a pair of basic projections $\prod_1$ and $\prod_2$ and defined as

$$DM = 1 + \beta(\prod_1 \circ f_2 - \prod_2 \circ f_1), \tag{5}$$

where β is a non-zero real parameter, $\circ$ represents composite mapping, $\prod_1$ expresses the object domain constraint set (convex), and $\prod_2$ is the Fourier domain constraint set (non-convex). $(\prod_1 \circ f_2 - \prod_2 \circ f_1)$ is the difference of the two projection operators, each composed with a map f_i: $E^N \to E^N$. Specifically, in Step 5, the complex amplitude stacks at different planes are back-propagated to the in-focal object plane. Then, these propagated complex amplitude stacks are synthesized in the Fourier domain to update the complex amplitude of the object. The recovery process is to enforce the known object $(\prod_1)$ and Fourier domain $(\prod_2)$ constraints through alternate projection as Eq. 5. While the system cannot be decoupled analytically, applying the two equations in turns for a few iterations was observed to be an efficient procedure to find the minimum.

2. Comparison of different QPI techniques

To clarify the advantages of the proposed HBDTI over the state-of-the-arts, we compare it with interferometric/non-interferometric QPI in Table S1. The classic interferometric digital holographic microscopy with synthetic aperture (DHM with SA) techniques can measure the high-resolution phase delay with at least 9 frames hologram via oblique [46, 50, 51] or structured illumination [43, 49, 52], achieving approaching incoherent diffraction limit resolution but having speckle noise and need phase unwrapping.

The typical non-interferometric methods including TIE [15, 16], differential phase contrast microscopy (DPC) [14, 55], and FPM [33, 34], can provide an effective alternative solution to QPI problems without complex optical alignment, highly coherent illumination, speckle noise and phase unwrapping. TIE demands a through-focus intensity stack with at least 3 frames to solve the axial intensity derivative [15, 16]. The existing TIE-related QPI approaches have consistently been implemented with BF illumination whose pattern is circle [18] or annulus [25], resulting in 2NA resolution limit [where illumination NA (NA_{ill}) is equal to objective NA (NA_{obj})] and low space-bandwidth product (SBP) [20].

DPC requires an intensity stack (at least 4 frames) at the in-focus plane with asymmetric illumination patterns to recover the missing frequency components induced by the anisotropy illumination [14, 55]. By employing the linearized WOTF-based model within BF illumination [17], the half-circle or half-annulus shaped pattern is usually implemented in DPC quantitative phase microscopy, resulting in incoherent diffraction limit and low SBP as well. FPM requires a variably illuminated in-focus intensity stack ($\sim$ 200 frames) including high-angle DF features [33, 34, 35, 36, 53, 54]. Combining ptychographic phase retrieval and coherent synthetic aperture, FPM enables high-SBP imaging that surpasses the incoherent diffraction limit at the cost of a large number of DF images, which are captured in low-SNR under the point illumination. In terms of matched illumination condition [37], DPC and FPM recover low-frequency components only when the illumination angles are matched to the cut-off angles allowed by the objective pupil function, which is critical for accurate phase recovery in non-interferometric QPI methods based on asymmetric illumination.

Table S1: Comparison of different QPI techniques.

Terms / **Techniques**	Raw data type (Typically)	Illumination pattern	Illumination mode	SBP	Key issues
DHM with SA	Hologram (9 frames) [46]	Oblique [46] or structured illumination [49]	Only BF	$<$ 5 megapixels	Approaching incoherent diffraction limit resolution; Speckle noise; Need phase unwrapping
TIE	Through-focus intensity stack (3 frames) [15]	Circle [18] or annulus [25]	Only BF	$\sim$ 5 megapixels	Incoherent diffraction limit; High-SNR; No matched illumination condition required [38]
DPC	Diverse illumination intensity stack (4 frames) [55]	Half-circle or half-annulus [55]	Only BF	$\sim$ 5 megapixels	Incoherent diffraction limit; High-SNR; Need matched illumination condition [37]
FPM	Diverse illumination intensity stack (200 frames) [33, 45]	Point [33]	BF & DF	$\sim$ 30.2 megapixels	Beyond the incoherent diffraction limit; Low-SNR; Need matched illumination condition [37]
HBDTI	Both BF and DF two through-focus intensity stacks (100 frames)	Discrete circle and complementary shape	BF & DF	$\sim$ 30.2 megapixels	Beyond the incoherent diffraction limit; High-SNR; No matched illumination condition

Different from the above state-of-the-arts, HBDTI captures two through-focus intensity stacks ($\sim$ 100 frames) under BF and DF illuminations. Due to discrete circle and complementary-shaped patterns rather than point sources, HBDTI can obtain high-SNR intensities, which is beneficial to ensuring high quality and robustness of phase retrieval results. By merging synthetic aperture and multiplexed illumination [46], the achievable resolution of HBDTI can beyond the incoherent diffraction limit for high-SBP imaging. Same with the situation of TIE, HBDTI bypasses the strict requirement of matched illumination condition through-focus scanning avoiding the missing of low frequency components [38].

To intuitively demonstrate the SBP capability among the above different QPI methods, the values in the column "SBP" in Table S1 are calculated based on the experimental parameters in the manuscript. Comparing the SBP corresponding to different QPI methods, Table S1 shows that HBDTI can achieve the same ability to reconstruct high SBP as FPM but with a relatively small amount of data, and its operation is simpler because without the need to consider the matched illumination condition. The above analysis indicates that to obtain the same SBP, FPM requires about 200 frames of variable-illuminated in-focus intensity stack, and HBDTI requires only about 100 frames of through-focus intensity stack under BF and DF illuminations. Moreover, to acquire the same SBP with a similar SNR, the exposure time for FPM is typically approximately 2.5 times (under BF illumination) to 10 times (under DF illumination) longer than that for the HBDTI method. Accordingly, HBDTI can perform the same SBP at a higher speed and higher dynamic range (better SNR) compared to the existing FPM method.

To verify the advantage of HBDTI using hybrid illumination in acquiring high-SNR intensity, we compared HBDTI with the traditional FPM method under a 9×9 LED array setup and the same exposure time of 55 ms per frame. FPM acquires a total of 81 in-focus intensity images as raw data through point-by-point illumination, whose recovered phase is shown in Fig. S1(a3). HBDTI collects 50 through-focus intensity images in BF and DF illumination, respectively, and its retrieved phase is shown in Fig. S1(b3). For better comparison, we normalized the dynamic display range of the BF intensity and DF intensity, respectively. The comparison between Figs. S1(a1) to S1(a2) and Figs. S1(b1) to S1(b2) shows that the dynamic range of BF and DF intensity in FPM differs by several orders of magnitude from HBDTI, and the SNR between corresponding intensity images is quite different as well. The intensity images acquired by HBDTI have better SNR with full advantage of the detector dynamic range. Under the same number of iterations, as shown

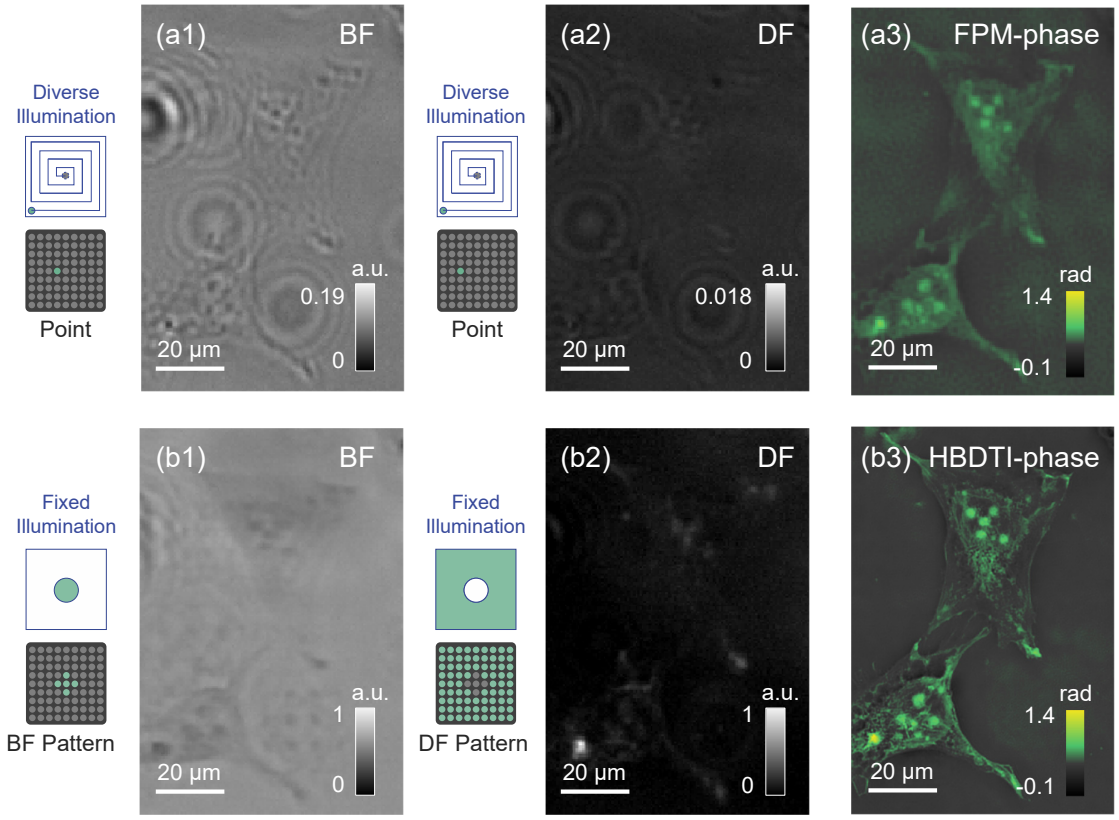

Figure S1: Comparison between quantitative phase imaging results of unlabeled HeLa cells corresponding to the traditional FPM method and that corresponding to the proposed HBDTI method. (a1), (b1) In-focus BF intensity of FPM and that of HBDTI, respectively. (a2), (b2) The in-focus DF intensity of FPM and that of HBDTI, respectively. (a3), (b3) The high-resolution retrieval phase of FPM and that of HBDTI, respectively.

in Figs. S1(a3) and S1(b3), the retrieval phase of HBDTI has less low-frequency noise and higher SBP than FPM, resulting from the captured high-SNR raw intensity images. It is verified that the proposed HBDTI method has higher accuracy and robustness of phase retrieval due to the higher dynamic range (better SNR) of input data.

3. Analysis of the data collection procedure

For reducing the number of measured intensity images and ensuring imaging quality, it is necessary to analyze the appropriate measurements scheme of HBDTI. Considering the theory of optimal frequency combination in TIE [56], the proper number of defocused images N_z is related to the defocus distance step z_{step}. Therefore, the suitable number of defocused images with different z_{step} under a certain number of iterations N_{iter} are analyzed to provide

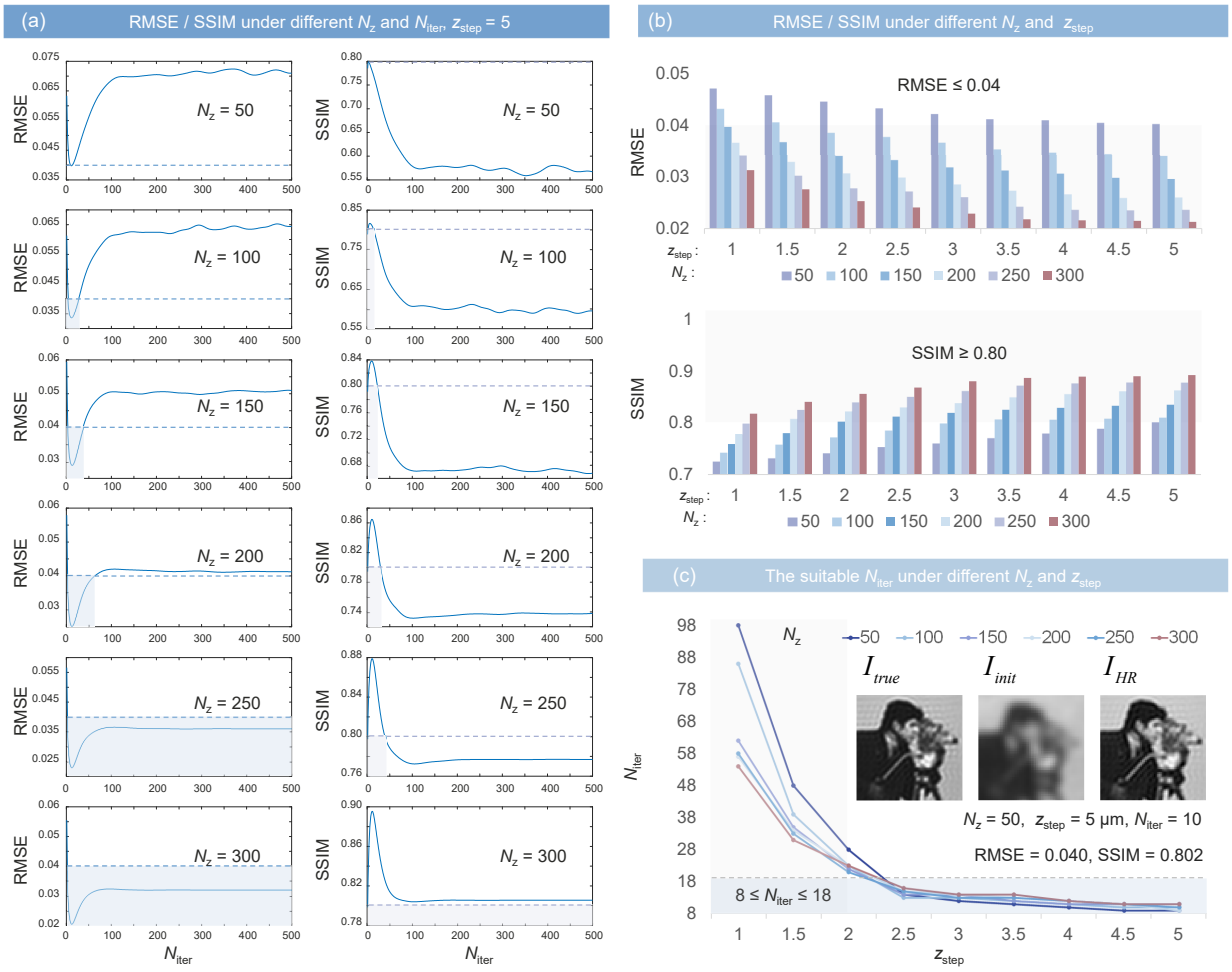

Figure S2: Simulation results of the absorbing object for analyzing the data collection procedure and the number of iterations. (a) RMSE and SSIM correspond to the retrieval results under different N_z and N_{iter}, $z_{step} = 5$ μm. (b) RMSE and SSIM correspond to the retrieval results under different N_z and z_{step}. (c) The suitable N_{iter} corresponds to the simulation results under different N_z and z_{step}.

an appropriate data collection procedure for experiments. The evaluation standards for measuring the imaging quality are the root mean square error (RMSE) (quantifies the overall difference between the true value and retrieved one) and the structural similarity index measure (SSIM) (quantifies the quality degradation caused by losses in high-frequency features). This section is still analyzed based on the simulation shown in Fig. 3 in the manuscript. Comparing the intensity images reconstructed under the various z_{step} and different N_z in Fig. S2, the corresponding recovery results have better quality when RMSE < 0.04, SSIM > 0.80. These values of RMSE $= 0.04$ and SSIM $= 0.80$ can be the critical point for evaluating image quality, which are used as a basis for adjudicating the suitable data collection procedure.

For the case of absorbing objects, it is illustrated in Fig. S2 that the suitable z_{step} is larger than 5 μm, and the appropriate N_z is 50. Based on the conclusion of absorbing objects, we focus on simulation and comparison of the reconstruction results under different N_z with $z_{step} = 5$ μm for the phase object case. As shown in Fig. S3, for phase objects, the reconstruct SSIM is far larger than 0.8, so the suitable standard here is changed to 0.9 (N_z is less than or equal to 150) and 0.93 (N_z is greater than 150). From the comparison between RMSE and SSIM parameters, similar conclusions can be drawn for phase objects. Thus, the proper parameter could be the case of $z_{step} = 5$ μm and $N_z = 50$ for absorbing objects and phase objects.

4. Analysis of the number of iterations

So as to further enhance the calculation efficiency and assure the imaging quality, we analyzed the iteration number N_{iter} for HBDTI. This section shows the suitable number of iterations N_{iter} under the appropriate z_{step} and N_z determined in Section 3. Here, the critical standards of the imaging performance are based on RMSE and SSIM. The SSIM value has a high weight in evaluation because it focuses on indicating the quality of high-frequency features, which is consistent with the core purpose of HBDTI to improve the retrieval resolution. It means that if there is no intersection between the N_{iter} ranges of RMSE and SSIM, the N_{iter} corresponding to the proper SSIM is the evaluation criterion.

Figure S2 reveals that when $z_{step} = 5$ μm, $N_z > 50$, the number of iterations corresponding to the suitable RMSE (RMSE < 0.04) and SSIM (SSIM > 0.80) are considered to be the suitable N_{iter} under the simulation results of the absorbing object. Figs. S2 and S3 exhibit that the N_{iter} can be selected as the minimum of the intersection of the above ten iterations. For the case of absorbing objects, there is no strong correlation between more iterations and good reconstruction quality, and the appropriate N_{iter} range is 10 to 20. For phase objects, larger number of iterations brings better retrieval performance but increases computational complexity. To enhance the computation efficiency while guaranteeing the imaging quality, the suitable parameter for phase objects should be the case of $N_z = 50$ and $N_{iter} = 182$ based on the simulation results in Fig. S3.

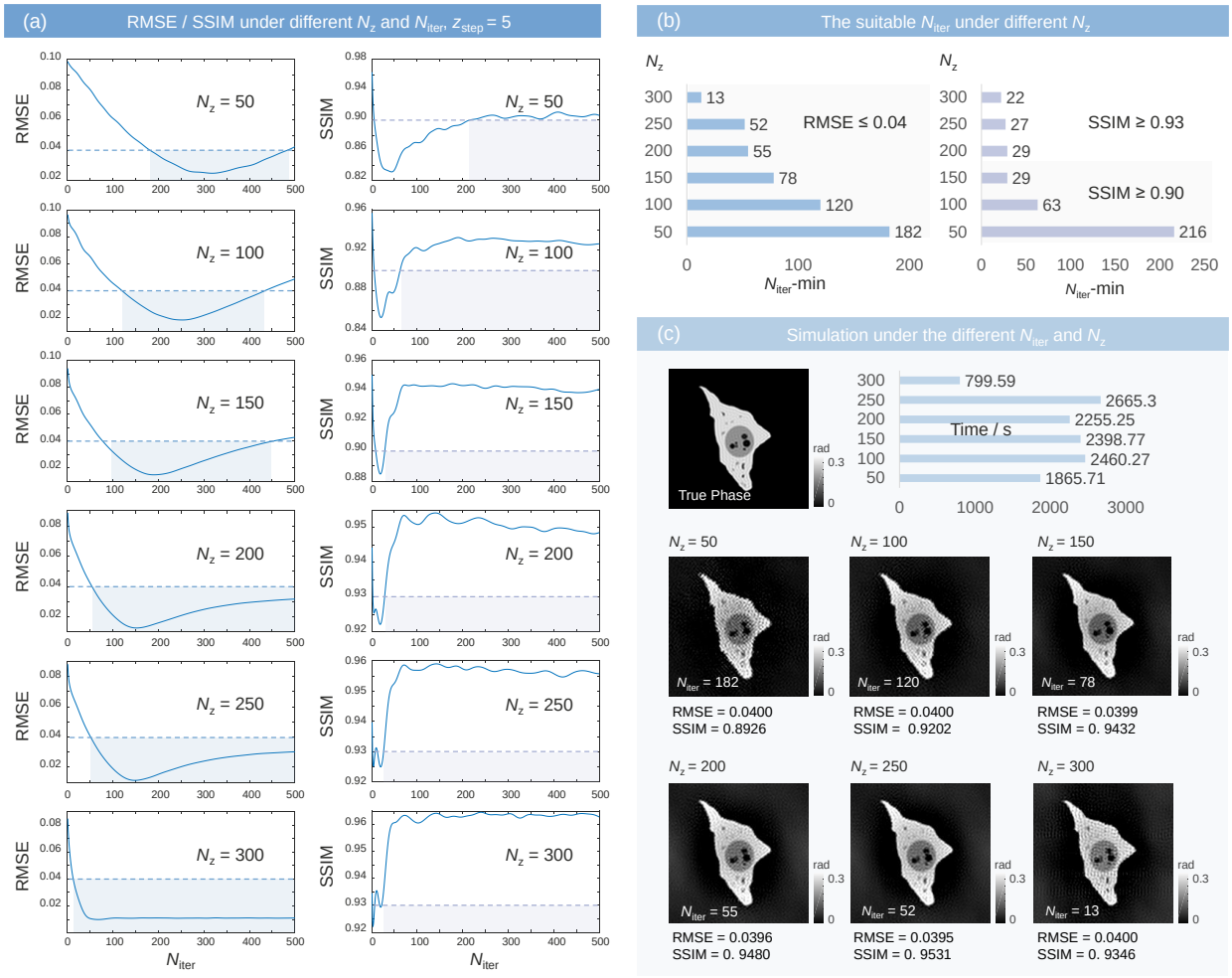

Figure S3: Simulation results of the phase object for analyzing the data collection procedure and the number of iterations. (a) RMSE and SSIM correspond to the retrieval results under different N_z and N_{iter}, $z_{step} = 5$ μm. (b) The suitable N_{iter} corresponds to the retrieval results under different N_z, $z_{step} = 5$ μm. (c) Simulation results under the different N_{iter} and N_z. Simulations are based on MATLAB R2016a using a personal computer with an Intel i7 CPU (no GPU).

5. LED illumination strategy

In the case of BF illumination, NA_{ill} is approximately equal to NA_{obj}, and the NA_{ill} corresponding to the DF imaging is larger than the NA_{obj}. Specifically, the BF intensity images of the specimen can be obtained by digitally matching the NA_{ill} to the NA_{obj} but without strictly matched illumination condition [38]. The DF intensity images can be attained by turning on the LEDs at the edge of the array, where the NA_{ill} is beyond the NA_{obj}. For example, the objective used in the experiments of the manuscript is $NA_{obj} = 0.16$, and the maximum effective NA in DF illumination corresponds to $NA_{ill} \approx 0.6$. In the experimental part of the manuscript, we used a central 9×9 LED array ($N_{LED} = 9$) with a distance $d_u = 2$ mm between adjacent units, which was placed $d_h = 12.3$ mm above the sample. The equivalent maximum NA_{ill} satisfies the following Eq. 6

$$NA_{ill} = \sin\theta = \sqrt{\frac{\left[\left(\frac{N_{LED}-1}{2}\right) \times d_u\right]^2}{\left[\left(\frac{N_{LED}-1}{2}\right) \times d_u\right]^2 + {d_h}^2}}. \tag{6}$$

When the number of rows or columns of LEDs (N_{LED}) is greater than 9 and d_h remains unchanged, the corresponding equivalent maximum NA_{ill} increases according to Eq. 6 and the theoretical limit resolution will be improved. The increase in the number of LEDs corresponding to DF imaging expands the maximum achievable imaging resolution, but the contributions of LED illumination from different angles will be effectively inversely solved at the cost of improving the number of defocused intensity images. In addition, it is not guaranteed that the maximum angular illumination component of the LEDs can be captured by the imaging detector due to the limitation of the mechanical hardware design of the optical microscope. Therefore, there is an upper limit to the number of N_{LED}, which needs to be considered according to the actual situation.

6. Quantification and analysis of HBDTI

To verify the ability of HBDTI to achieve accurate phase retrieval, the experiment based on a micro-lens array (SUSS MicroOptics, Nr. 18-00036, pitch = 30 μm, ROC = $9.67mm \pm 5\%$) was implemented (shown in Fig. S4). The quantitative phase result of the micro-lens array reconstructed based on HBDTI is shown in Fig. S4(a) and the corresponding single micro-

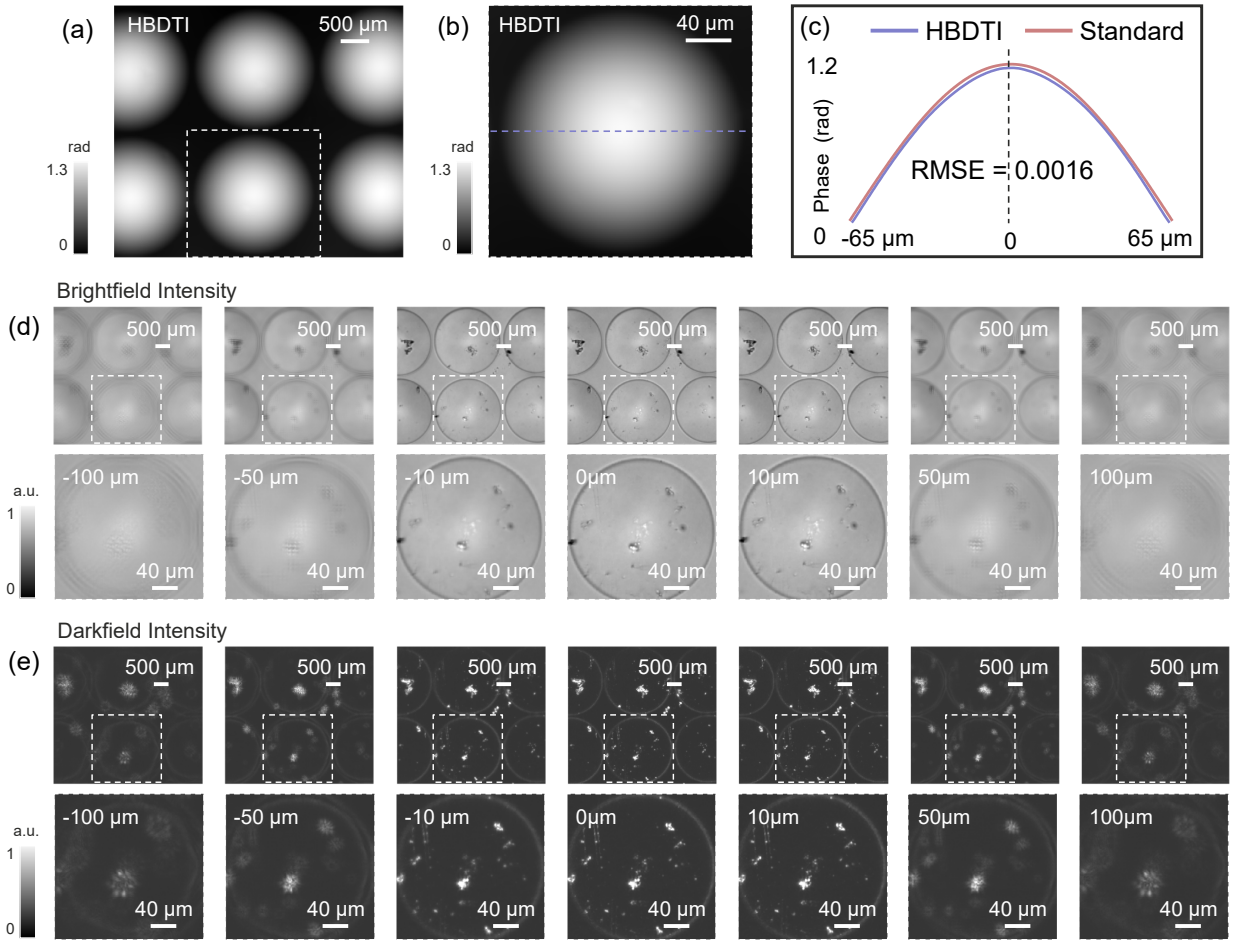

Figure S4: Quantitative phase imaging result of the micro-lens array. (a) The retrieval phase of micro-lens array based on HBDTI. (b) Enlarged view of a single micro-lens array corresponding to the white dashed box in (a). (c) Profile corresponding to the blue dashed line in (b). (d), (e) Through-focus intensity stacks of micro-lens array collected under BF and DF illumination (with defocus distances of ±100μm, ±50μm, ±10μm, and 0 μm as examples, and 0 μm corresponds to the in-focus case).

lens enlarged in Fig. S4(b) has a clear profile and complete low-frequency components. As illustrated in Fig. S4(c), HBDTI correctly recovered the profile across the center of a single lens in Fig. S4(b). It means that the lens profile recovered by HBDTI is in good accordance with the manufacturer's specifications, verifying its ability to achieve accurate phase retrieval.

Instead of introducing measurement diversity through different illumination angles in FPM, the HBDTI method artificially introduces hybrid illumination and intensity transport as prior knowledge, to modulate essential information of the scene into the original image signal by z-axis scanning. The basic idea of phase retrieval based on intensity transport is to generate phase contrast via introducing defocusing on the pupil plane, thereby converting phase information into intensity image. When an off-axis point source illuminates an object, the final imaged position of the origin is displaced incrementally laterally with increasing defocus distance. Under BF and DF illuminations, the condenser aperture diaphragm is an extended incoherent area source of finite size. As the defocus distance increases, the size of the speckle produced by the source increases proportionally, creating a uniform circular spot with a lateral radius proportional to the defocus distance, thereby introducing distinct features to captured intensity. The through-focus intensity stacks of micro-lens array collected under BF and DF illuminations are shown in Fig. S4(d) and Fig. S4(e). We normalized the dynamic display range of the BF intensity and DF intensity, respectively, for better visual quality. Fig. S4(d) and Fig. S4(e) exhibit that the HBDTI method can introduce measurement diversity to the captured images through illumination modulation and defocusing operations.

7. HBDTI MATLAB source code and datasets

A. Overview of HBDTI MATLAB code

Supplementary codes and dataset contain two folds (the "Data" folder, the "Func" folder), three MATLAB files (∗.m) and one TEXT file (∗.txt) (Fig. S5).

- The "Data" folder includes one image named "TIE" (∗.tif) that can be used to generate raw data.
- The main function files of "Func" folder include:

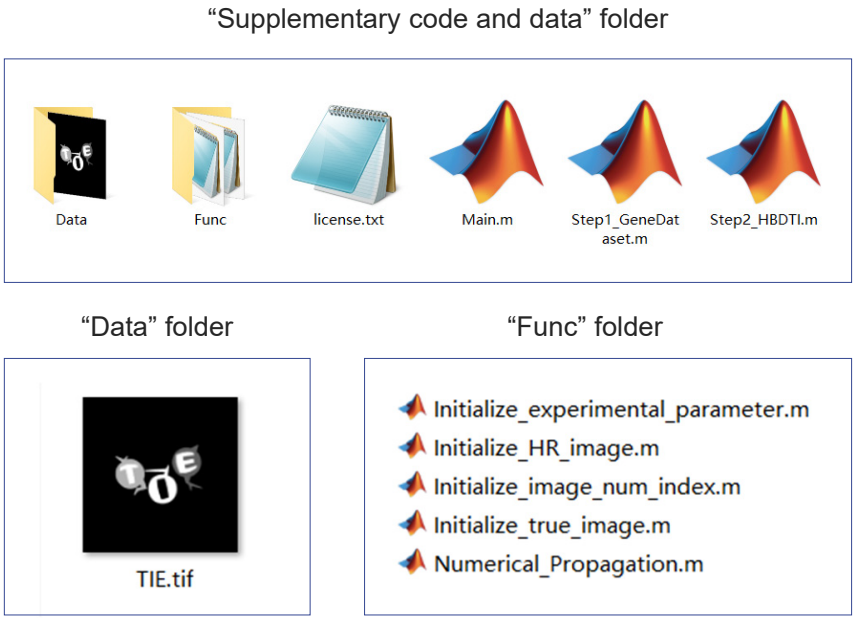

Figure S5: The “Supplementary code and data” directory.

- Initialize_experimental_parameter.m: codes for initializing the experimental parameters.
- Initialize_HR_image.m: codes for initializing the high-resolution image.
- Initialize_image_num_index.m: codes for initializing the image index under the LED illumination model.
- Initialize_true_image.m: codes for initializing the true image for quantitative evaluation.
- Numerical_Propagation.m: codes for numerical propagation the complex field to another plane at a given distance using “Angular Spectrum” or “Fresnel” method.

- The file “Main.m”: demo codes for generating the dataset and implementing the entire HBDTI process, including two steps: “Step1_GeneDataset.m” and “Step2_HBDTI.m”.
- The file “Step1_GeneDataset.m”: demo codes for generating the defocus intensity stacks under BF and DF illumination based on the Abbe imaging principle, which is used as the input data of “Step2_HBDTI.m”.
- The file “Step2_HBDTI.m”: demo codes for implementing the entire HBDTI super-resolution process, including the initial guess, numerical propagation, intensity constraints for image reconstruction iterative process.

- The file "License.txt" is our copyright notice for the data codes.

B. User guide for the HBDTI MATLAB code

B1. System parameter setting

Before running the demo codes ("Step2_HBDTI.m"), it is necessary to set the system parameters, which include (Fig. S6):

- LED array number
- Distance from LED to Stage
- Distance between adjacent LED units
- Illumination wavelength of LED
- Objective magnification
- Objective numerical aperture (NA)
- Camera pixel size

```
% System paras LED and Camera
LED_num_x = 9;                          % LED array number
LED_num_y = 9;                          % LED array number
LED2stage = 120e3;                      % Distance from LED to Stage
LEDdelta = 6.5e3;                       % Distance between adjacent LED units
Lambda = 0.6354;                        % Illumination wavelength of LED
LED_center = (LED_num_x*LED_num_y+1)/2;

% System paras objective
Mag = 4;                                % Objective magnification
NA = 0.1;                               % Objective numerical aperture (NA)
Pixel_size = 5.5/Mag;                   % Camera pixel size
M = 64;                                 % Raw image size
N = 64;
```

Figure S6: Code for setting the system parameters.

For detailed system parameters are described in the file Initialize_experimental_parameter.m.

B2. Experimental parameter setting

Before running the demo codes ("Step2_HBDTI.m"), it is necessary to set the system parameters, which include (Fig. S7):

- Number of defocused intensity images
- Step size of adjacent defocused intensity images
- Wave vector
- Upsampling rate of the initial guess

```
% Initialize experimental parameter
z_num = 400;                          % Number of defocused intensity images
z_step = 0.5;                         % Step size of adjacent defocused intensity images
k = 2*pi/Lambda;                      % Wave vector
Mag_image = 3;                        % Upsampling rate
kmax = 1/Lambda*NA;
```

Figure S7: Code for setting the experimental parameters.

For detailed system parameters are described in the file Initialize_experimental_parameter.m.

B3. Raw images generating

Based on the set parameters, the raw images for HBDTI can be generated by running the file "Step1_GeneDataset.m".

- The in-focus complex amplitudes corresponding to different LED illumination angles are generated from the simulated high-resolution image (Fig. S8).
- Using the in-focus complex amplitude stacks, the new complex amplitude stacks with different defocus distances can be obtained through numerical propagation.
- Based on the principle of incoherent superposition, the corresponding through-focus intensity stacks can be generated by the above complex amplitude stacks under BF and DF illumination, respectively, providing the input data (I_allb.mat and I_alld.mat) for the HBDTI algorithm (Fig. S9).

```
%% Generate all sub-images of complex amplitudes corresponding to different defocus distances
figure
for num = 1: LED_num_x*LED_num_y
    kx = round(kxky_index(num,1));
    ky = round(kxky_index(num,2));
    F_Hi_resshow = F_Hi_res;
    Subspecturm = F_Hi_res(Fcenter_Y+ky-fix(M/2): Fcenter_Y+ky+ceil(M/2)-1, Fcenter_X+kx-fix(N/2):Fcenter_X+kx+ceil(M/2)-1);
    Subspecturm = Subspecturm.*Aperture_fun;
    F_Hi_resshow(Fcenter_Y+ky-fix(M/2): Fcenter_Y+ky+ceil(M/2)-1, Fcenter_X+kx-fix(N/2):Fcenter_X+kx+ceil(M/2)-1) = Subspecturm;

    subplot(1,2,1)
    imshow(log(abs(F_Hi_resshow)+1),[]);
    title('Raw Subspecturm');
    pause(0.01)
    U = (ifft2(fftshift(Subspecturm)));

    for z = 1:z_num
        Uz = Numerical_Propagation(U,(z-1).*z_step,Pixel_size,Lambda,'Angular Spectrum');
        Uall{num,z} = Uz;
        subplot(1,2,2)
        imshow(abs(Uz),[]);title(num);
        pause(0.03)
    end

    num;
end
```

Figure S8: Code for generating the in-focus complex amplitudes corresponding to different LED illumination angles.

B4. Image reconstruction based on HBDTI

After initializing the related parameters and loading the raw images, image reconstruction can be performed based on four steps:

- Initial guess: based on the file of Initialize_HR_image.m to initialize the high-resolution image with the upsampling rate (Fig. S10).
- Numerical propagation: a series of high-resolution defocused intensity stacks are obtained through numerical propagation under corresponding LED illumination angles.
- Intensity constraints: the calculated low-resolution intensities after the downsampling of pixel binning can be treated as the input of the following intensity constraints process (Fig. S11).
- Image reconstruction iterative process based on difference map: the complex amplitude stacks at different planes are back-propagated to the in-focal object plane and then these propagated complex amplitude stacks are synthesized in the Fourier domain

```
%% Add all sub-images to generate brightfield intensity images
for z = 1:z_num
    I = 0;
    scale = 1;
    for num = 1: 9
        %% brightfield image
        I = I + abs(Ua11{num,z}).^2/scale;
    end
    I_a11b{z}=I;
    imshow(I_a11b{z},[]);title('add all sub-images for brightfield intensity');
    pause(0.01)
end
save I_a11b I_a11b


%% Add all sub-images to generate darkfield intensity images
for z = 1:z_num
    I = 0;
    scale = 1;
    for num = 10: LED_num_x*LED_num_y
        %% darkfield image
        I = I + abs(Ua11{num,z}).^2/scale;
    end
    I_a11d{z}=I;
    imshow(I_a11d{z},[]);title('add all sub-images for darkfield intensity');
    pause(0.01)
end
```

Figure S9: Code for generating the through-focus intensity stacks under BF and DF illumination, respectively.

to update the object complex amplitude (Fig. S12). Fig. S13 illustrates the high-resolution image acquired by HBDTI.

```
%% Initialization
eval Initialize_experimental_parameter;
eval Initialize_HR_image;
eval Initialize_ture_image;
eval Initialize_image_num_index;
```

Figure S10: Code for initializing parameters.

```
%% simulate defocus brightfield intensity for intensity constraints
I_now = 0;
for num = 1: 9
        U{num}   = Numerical_Propagation(U{num}, z_step, Pixel_size, Lambda, 'Angular Spectrum');
        I_now = I_now + abs(U{num}).^2;
end
for num = 1:  LED_num_x*LED_num_y
    U{num}   = U{num}.*sqrt(I_allb{z}./I_now);
end

%% simulate defocus darkfield intensity for intensity constraints
I_now = 0;
for num = 10: LED_num_x*LED_num_y
        U{num}   = Numerical_Propagation(U{num}, z_step, Pixel_size, Lambda, 'Angular Spectrum');
        I_now = I_now + abs(U{num}).^2;
end

for num = 10: LED_num_x*LED_num_y
        U{num}   = U{num}.*sqrt(I_alld{z+1}./(I_now+eps));
end
```

Figure S11: Code for intensity constraints process.

```
%% Image reconstruction based on difference map
if(z == z_num)
    for num = 1 : LED_num_x*LED_num_y
        kx = round(kxky_index(num,1));
        ky = round(kxky_index(num,2));

        Subspecturmcorrected = fftshift(fft2(U{num})).*conj(Aperture_fun);
        F_change(Fcenter_Y+ky-fix(M/2): Fcenter_Y+ky+ceil(M/2)-1, Fcenter_X+kx-fix(N/2):Fcenter_X+kx+ceil(M/2)-1) = Subspecturmcorrected;
        Fup = Fup + F_change;

        Aperturelarge_change(Fcenter_Y+ky-fix(M/2): Fcenter_Y+ky+ceil(M/2)-1, Fcenter_X+kx-fix(N/2):Fcenter_X+kx+ceil(M/2)-1) = Aperture_fun;
        Fdown = Fdown + abs(Aperturelarge_change).^2;
    end
    F = Fup./(Fdown+eps);

    Result = ifft2(fftshift(F));
    I_cal = abs(Result.*Result);
```

Figure S12: Code for the image reconstruction process.

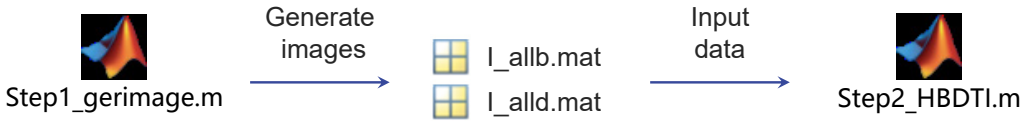

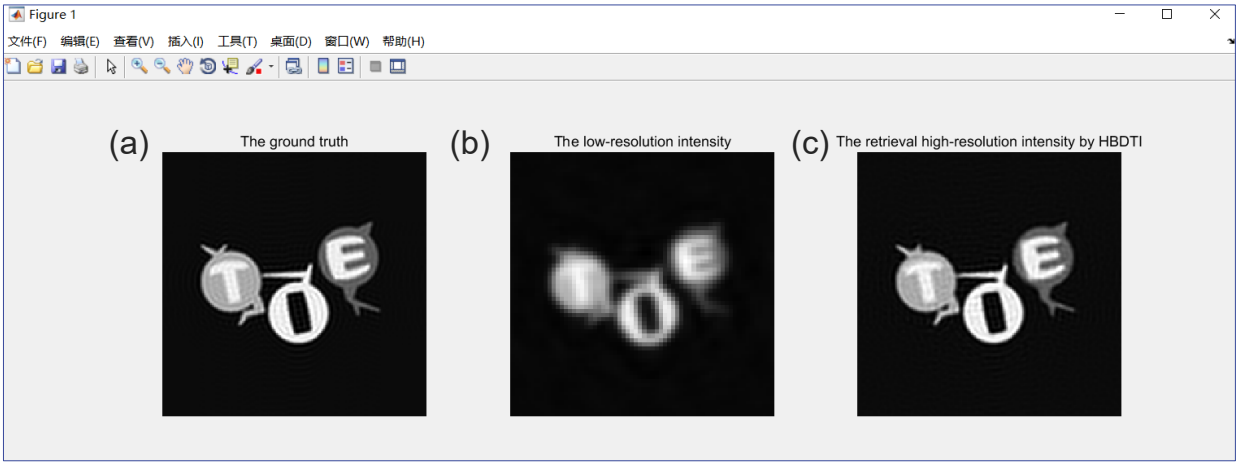

Figure S13: (a) The ground truth image. (b) The low-resolution image of in-focus BF intensity. (c) The high-resolution image acquired by HBDTI via running the main program.